Noise Due to Interaction of Boundary-Layer Turbulence with a Compressor Rotor

N. Moiseev,* B. Lakshminarayana,† and D. E. Thompson‡
Applied Research Laboratory, Pennsylvania State University, State College, Pa.

The radiated sound due to a compressor or propulsor rotating blade row was investigated under various operating conditions and inflows. The propulsor was operated in air with different blade space-to-chord ratios, different flow coefficients and differing turbulence (nonisotropic) inflows. The inflows ingested were: 1) the natural boundary layer on the hub and annulus wall, 2) a tripped boundary layer on the hub, and 3) a fully developed boundary layer on the hub. The turbulence properties were also altered by placing a grid at the inlet. The mean velocity profiles, turbulence intensities, length scales, and energy spectra of the inflow, as well as near- and far-field acoustic spectra, were measured. A parametric investigation of the effect of inflow characteristics on the radiated sound was made. Several length scales were found to exist simultaneously. The noise due to small scale turbulence seemed to depend on the ratio of the square of the turbulence velocity normal to the blade divided by the axial length scale. The long eddies (compared to blade spacing) were primarily responsible for discrete tone production.

Nomenclature

ABL,NBL,FDBL = artificial, natural, and fully developed boundary layer, respectively
B = number of blades
c = blade chord
C_L = lift coefficient based on the cascade mean velocity
$E_{u_iu_j}(k)$ = spectrum function of turbulence kinetic energy
k = wave number
L_x, L_θ = axial integral length scale (TU_x) and tangential integral length scale, respectively
$(\overline{q^2})^{1/2}$ = turbulence velocity (rms value) normal to blade chord
r_T = tip radius of rotor
r, θ, x = radial, tangential, and axial coordinates, respectively
S = local blade spacing $2\pi r/B$
T = integral time scale
u = fluctuating velocity in the axial direction
U_c = axial mean velocity at midradius
U_{rel} = $(U_x^2 + U_T^2)^{1/2}$, flow velocity relative to rotor
U_T = velocity of rotor blade
U_x = axial mean velocity
v = fluctuating velocity in the circumferential direction
$\rho_{uu}(\tau)$ = $\overline{u(x,r,\theta,t)\,u(x,r,\theta,t+\tau)}/\overline{u^2}$
$\rho_{vv}(\theta)$ = $\overline{v(x,r,t,\theta)\,v(x,r,t,\theta+d\theta)}/\overline{v^2}$
ϕ = flow coefficient $U_x/(U_T)_{\text{tip}}$
τ = delay time, s

Introduction

TURBULENCE is an important cause of noise generation in aircraft turbomachinery (propellers, fans, and compressors) as well as marine vehicles (propulsors and ventilation fans). The interaction of turbulence with the potential flowfield of the rotor results in quadrupole noise sources. Dipole sources result from the random fluctuations in pressure distribution caused by the random fluctuations in the angle of attack due to the turbulence.

Recent investigations[1,2] have revealed that inlet turbulence, both in the freestream and hub or annulus wall boundary layers, is a major source of noise in compressors, fans, and propulsors. Additional turbulence is generated in the wakes of inlet guide vanes (aircraft) or control surfaces (marine). In one of these earlier studies,[2] a detailed investigation of the radiated sound due to nearly isotropic turbulence interacting with a rotor was carried out. The aim of the investigation was to study the empirical relationship between turbulence intensity and length scales and the radiated sound pressure. A second aim was to check the validity of theories developed by Mani[3] and Sevik[4] which predict the radiated sound due to isotropic and homogeneous turbulence.

A review of the major sources of turbulence and its effect on noise in aircraft, marine, and industrial turbomachinery as well as an up-to-date review of the various theoretical and experimental investigations is described in Ref. 5. A more general review of all sources of noise is given in Ref. 6.

The relationship between the inlet turbulence properties (such as intensity, length scales, and energy spectrum) and the radiated sound is not fully understood. The objective of this research program was to carry out a systematic study to determine experimentally how the radiated sound depends on these turbulence characteristics. This study was carried out for three different inlet boundary layers at the design flow coefficient of the turbomachine and at three flow coefficients with one type of boundary layer, all with and without a grid. Two rotor blade solidities were considered and both the near- and far-field radiated sound were studied. The operating variables provided a wide range of turbulence eddy sizes leading to an understanding of the role played by the turbulence integral scale on noise generation.

Turbomachinery Noise Facility

An existing aeroacoustic facility, as described in Ref. 2 was modified by adding a long inlet duct and stationary hub to permit formation of a boundary layer. The facility consists of four main components as shown in Fig. 1: an anechoic chamber surrounding the inlet, the test rotor, a sound-assorbing chamber downstream of the rotor, and Joy Axivane fan to provide airflow.

Presented as paper 76-568 at the 3rd AIAA Aero-Acoustics Conference, Palo Alto, Calif., July 20-23, 1976; submitted Aug. 20, 1976; revision received Aug. 29, 1977.

Index categories: Aeroacoustics; Airbreathing Propulsion; Marine Propulsion.

*Graduate Assistant.
†Professor of Aerospace Engineering. Associate Fellow AIAA.
‡Research Associate.

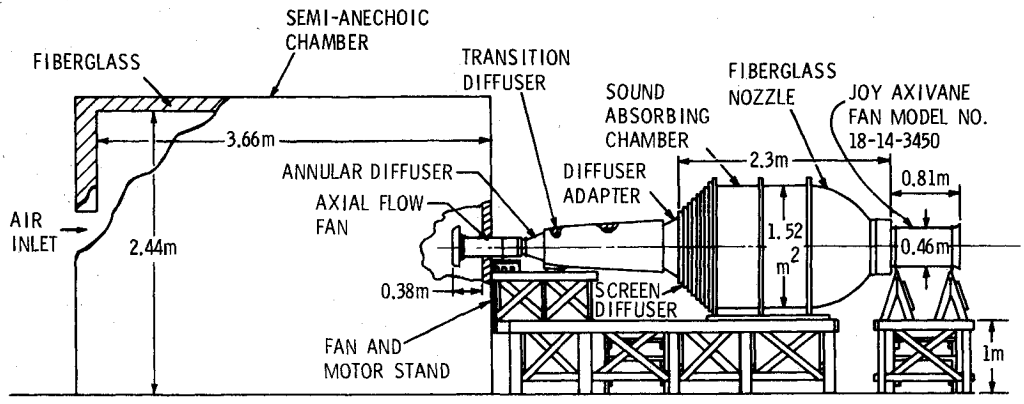

Fig. 1 Turbomachinery noise facility and the anechoic chamber.

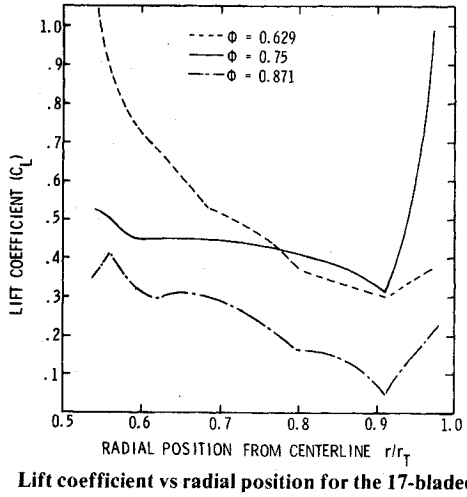

Fig. 2 Lift coefficient vs radial position for the 17-bladed rotor.

The anechoic chamber has inside dimensions of $3.35 \times 3.66 \times 2.44$ m. Construction is a wooden frame with walls much like a bookcase; the spaces between the shelves being filled with Owens-Corning Type 705 industrial fiberglass. The floor is covered with the same material. Fiberglass was suspended from the frame in wire baskets forming the ceiling. The fiberglass treatment is 15.24 cm thick with a 2.54-cm airspace between the fiberglass and exterior wall. The rotor inlet protrudes 0.38m through the center of a 3.35×2.44 m wall. An air inlet hole, 1.4 m in diameter was cut in the opposite wall and covered with a sheet of porous plastic foam to filter out dirt. The chamber was calibrated in the above configuration by driving a speaker with pure tones between 0.1 and 20 kHz. The variation of sound pressure level with distance from the centerline of the inlet followed the inverse square law. The result was that the chamber was anechoic over the range tested.

Two rotors were employed in the investigation – one having 10 blades and one having 17 blades. Each rotor (design details in Ref. 7) had identical blades with two differing solidities. The hub-to-tip ratio of the rotor blades was 0.482, with a tip diameter of 17.53 cm. The chord length was nearly constant from hub to tip at 4.06 cm. The stagger angle varied from 0.31 rad at the hub to 0.81 rad at the tip. The rotor was of free vortex design. The midspan blade spacing for the 17- and 10-bladed rotors were 2.43 cm and 4.13 cm, respectively. The range of mean velocities at the rotor inlet was 39.0 to 51.2 m/sec for all the tests carried out. At design, the lift coefficient for the 17-bladed rotor was 0.46 and the flow coefficient was 0.75.

A plot of experimentally determined C_L vs radial position is given in Fig. 2 for the 17-bladed rotor. The operating conditions were as follows: $\phi = 0.629$ at 6810 rpm and 39.3 m/s, $\phi = 0.75$ at 5440 rpm and 39 m/s, and $\phi = 0.871$ at 5440 rpm and 51.2 m/s.

Experimental Method and Instrumentation

Aerodynamic Measurements

Measurements of the mean velocity and the turbulence intensity in both the axial and tangential directions at the inlet were made with an X-configuration hot-wire probe. Standard hot-wire data acquisition techniques were used in conjunction with a correlation computer and spectrum analyzer to derive turbulence characteristics. The recorded ac signals are accurate down to dc values, since there was no signal filtering. Hence, the correlation measurements were accurate, including the calculation of long-length scales. The probe was traversed radially along the blade span; measurements were taken at different radial locations at a position two chord lengths upstream of the rotor (as shown in Fig. 3a). Mean velocity measurements were made using a hot-wire probe at 90- and 180-deg separation from the main measuring station to determine if the flow was axisymmetric. The entry flow was axial everywhere upstream of the rotor.

The axial velocity and, therefore, flow coefficient were controlled by the Joy axial-flow fan, located downstream of the rotor as shown in Fig. 1. An artificial boundary layer (ABL) was created by tripping it with a 0.318-cm-thick O-ring on the hub immediately behind the nose cone as shown in Fig. 3b. In addition, a fully developed boundary layer (FDBL) was produced by coating the hub with rough sandpaper and removing the nose cone as shown in Fig. 3b. The turbulence properties were altered by placing a square mesh grid at the inlet 3.5 diameters upstream of the rotor (see Fig. 3a). The grid had a mesh size of 2.86 cm and a rod diameter of 0.556 cm. Experiments were carried out with and without this grid. The axial length scales of the turbulence were derived by using an X-array hot-wire probe in conjunction with a correlation computer and an *x-y* plotter to obtain autocorrelation curves for the axial component of the velocity fluctuations. Then, using the equation

$$\int_0^\infty \rho_{uu}(\tau)\,d\tau = T \tag{1}$$

the temporal integral scale was derived from the autocorrelation curve. This time scale multiplied by the local axial velocity gives the axial integral length scale (L_x).

The circumferential length scales were determined by using two X-array hot-wire probes whose angular separation could be varied. The cross-correlation between the circumferential components of turbulent fluctuations at various angular separations, with axial and radial location held constant, of the hot-wire probes was computed with the correlation computer and plotted as correlation coefficient normalized by $\overline{v^2}$ versus angular separation in degrees. Details of the flow instrumentation, technique and the hot-wire equation are given in Ref. 7. The integral length scales were derived from this plot using the equation

$$r\int_0^\infty \rho_{vv}(\theta)\,d\theta = L_\theta \tag{2}$$

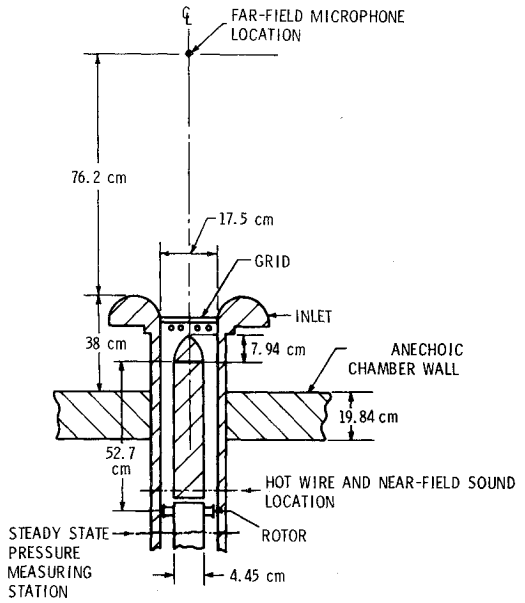

Fig. 3a Plan view of inlet showing measuring stations.

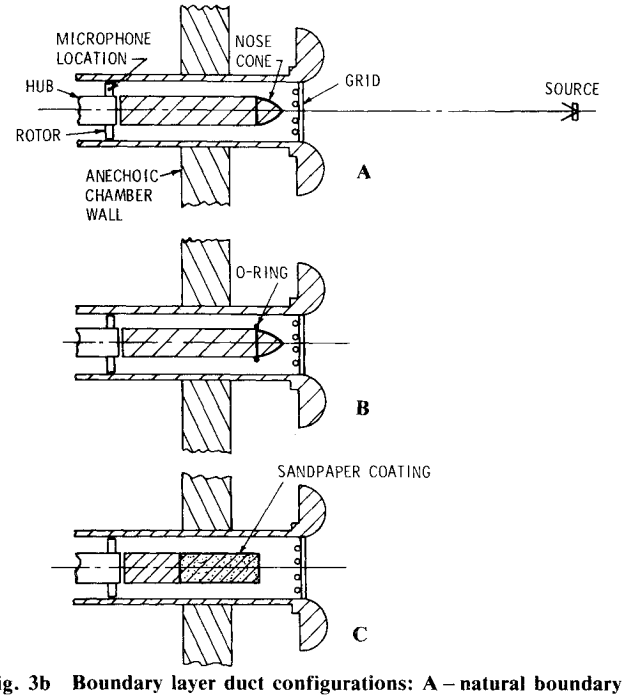

Fig. 3b Boundary layer duct configurations: A – natural boundary layer, B – artificial boundary layer, and C – fully developed boundary layer.

The length scales were determined at each of five radial positions (described later) for all three boundary layers at the design flow coefficient, with and without the grid installed. In addition, turbulent energy spectra were obtained for both the axial and circumferential components of the fluctuating velocity at each radial location. It was assumed that the inflow turbulence characteristics did not change with rotor geometry, and hence no turbulence measurements were carried out for the 10-bladed rotor.

Acoustic Measurements

Measurements of the radiated sound were made at two locations: 1) two chords upstream of the rotor, called the near field, and 2) 4.35 duct diam upstream of the inlet duct opening inside the anechoic chamber, labeled the far field, as shown in Fig. 3a. The near-field measurements were made with the microphone mounted flush in the wall of the duct.

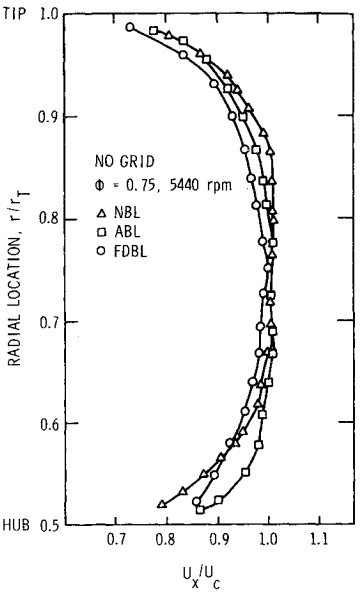

Fig. 4 Mean axial velocity profiles.

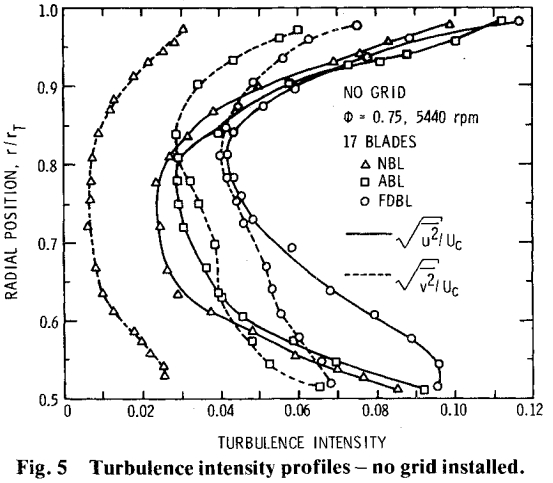

Fig. 5 Turbulence intensity profiles – no grid installed.

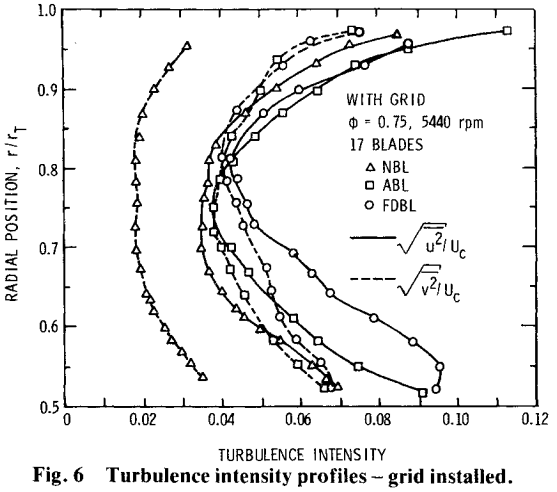

Fig. 6 Turbulence intensity profiles – grid installed.

The sound spectra were obtained by analyzing the ¼-in. B&K microphone signal through a Spectral Dynamics real-time spectrum analyzer and recorded with an *x-y* plotter.

Spectra were obtained for three different flow coefficients, 0.75, 0.871, and 1.03, without the grid for NBL and for three different boundary layers at the design flow coefficient ($\phi = 0.75$) with and without the grid. All sound measurements

Table 1 Experimental variables and BPF tone levels

Number of blades	Boundary layer	Grid	Flow coefficient	U_c, m/s	10-bladed BPF tone level SPL, dB	17-bladed BPF tone level SPL, dB
17	Natural	No	1.03	51.5	...	79.0
17	Natural	No	0.871	43.5	...	79.0
10, 17	Natural	No	0.75	39.0	81.4	79.0
10, 17	Natural	Yes	0.75	39.0	79.4	74.7
10, 17	Artificial	No	0.75	39.9	79.0	79.9
10, 17	Artificial	Yes	0.75	39.9	74.4	74.2
10, 17	Fully dev.	No	0.75	39.5	84.7	82.7
10, 17	Fully dev.	Yes	0.75	39.5	75.3	80.0

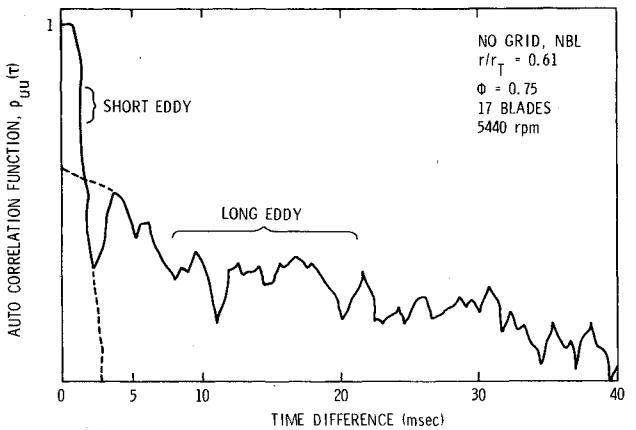

Fig. 7a Typical autocorrelation curve for no grid showing two scales.

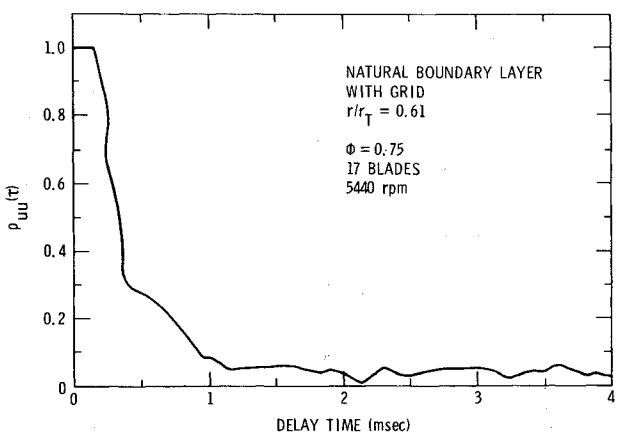

Fig. 7b Typical autocorrelation curve for grid installed.

were performed with the 10-bladed, as well as the 17-bladed, rotor configuration.

Because of the length of the duct and its possible influence on sound propagation, calibration of the acoustic response of the duct for all duct configurations was performed. The results were identical for every configuration. The sound spectra have *not* been corrected for the duct acoustic response.

The variables used in the experimental program and the measurement program for each of the variables are shown in Table 1. The design flow coefficient $\phi = 0.75$ corresponds to an inflow velocity of 39 m/s. Unless otherwise stated, the rotor was operated at a constant speed of 5440 rpm.

Experimental Results

Aerodynamic Measurements

The results of axial mean velocity measurements are shown in Fig. 4. The artificial boundary layer (ABL) is seen to have

Table 2 Axial integral length scales (cms)

r/r_T	No grid Long	No grid Short	No grid Average	Grid
	Natural boundary layer (NBL)			
0.52	86	10	46	1.5
0.61	68	7	42	2.2
0.75	90	9	77	1.9
0.88	97	12	68	2.2
0.97	117	5	81	2.2
	Artificial boundary layer (ABL)			
0.52	386	69	321	1.9
0.58	121	14	74	1.7
0.70	84	13	54	0.9
0.84	194	45	160	1.0
0.97	152	40	112	3.2
	Fully developed boundary layer (FDBL)			
0.52	164	21.0	112.0	2.1
0.58	NP	2.0	2.0	2.1
0.70	34	3.0	5.0	1.5
0.84	NP	1.4	1.4	0.4
0.97	85	13.0	70.0	1.0

NP = not present.

nearly the same thickness as the natural boundary layer (NBL) but has a much steeper gradient at the hub. The fully developed boundary layer (FDBL) is thicker than either the NBL or ABL. A logarithmic plot of velocity profile seems to indicate that all three boundary layers obey the "law of the wall."[7]

In Figs. 5 and 6, the turbulence intensity profiles are shown for all three boundary layers. The levels increase with increasing boundary-layer thickness, with the maximum intensities for FDBL case. The turbulence intensities with the grid are generally higher. For the NBL, the tangential component ($\sqrt{\overline{v^2}}/U_c$) of turbulence is much lower than the axial component ($\sqrt{\overline{u^2}}/U_c$). For the ABL and FDBL, the two components of turbulence intensity are nearly the same for the middle third of the passage. The tangential component is lower than the axial component inside the hub and annulus wall boundary layers. Hanson's measurements[1] indicate that, for a fan operating in atmospheric turbulence, the contraction of the eddies at the inlet would result in larger values of the tangential component of turbulence intensity than of the axial component. These results have not been confirmed by our measurements.

For the axial component of the velocity fluctuations, two length scales were found to exist simultaneously for the no-grid condition for all three boundary layers. Figure 7a is a typical autocorrelation curve with no grid installed showing evidence of two length scales. The short eddy has a small time scale as seen near the origin (extrapolated by dotted curve) of Fig. 7a. The length scale of this eddy was determined using this curve and Eq. (1). Similarly the larger eddy has a large time scale, as indicated in Fig. 1, extrapolated near the origin

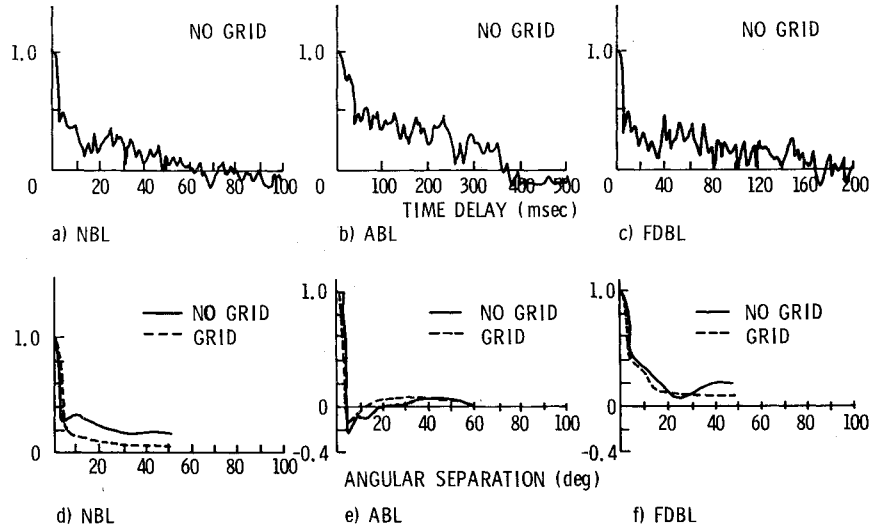

Fig. 8 Correlation curves, each boundary layer, $r/r_T = 0.52$, $\phi = 0.75$, 17 blades, 5440 rpm.

by dotted lines. This curve, along with Eq. (1), was used to determine the long length scale. The evidence of two length scales also appears in the circumferential spatial cross-correlation with the grid; it disappears for the autocorrelation (see Fig. 7b). This indicates that the grid reduces the axial length scale drastically, but has no effect on the circumferential length scale.

In Table 2, the axial length scales found at five radial locations are given for each of the three boundary layers. It is readily seen that two scales were found at all locations for the no-grid condition except for two locations for the FDBL.

The NBL shows the greatest uniformity for axial length scales with no grid installed. The FDBL shows the greatest variation. These variations are smoothed out by the installation of the grid. All three boundary layers have axial scales of the same order of magnitude with the grid installed. Table 2 also gives the average axial integral length scales. These scales were derived using Eq. (1) as previously discussed. Instead of splitting the autocorrelation curve into two curves as shown in Fig. 7a, the entire autocorrelation curve was integrated.

Table 3 gives the circumferential length scales at five radial locations for all three boundary layers. Two scales were present for all locations and boundary layers; however, not all could be calculated.

Figures 8 and 9 show the correlation curves near the hub with various entry boundary layers at $\phi = 0.75$ for $r/r_T = 0.52$ and 0.58, respectively. The autocorrelation, $\rho_{uu}(\tau)$, is shown only for the no-grid case and the cross-correlation for both the cases. The correlations are highly anisotropic in all these cases. (Please see Ref. 7 for correlation curve at all other locations.)

A possible explanation for the presence of two turbulence length scales is the fact that the eddies in the freestream are stretched as they are ingested into the inlet, resulting in elongated eddies. Small scale eddies arise from the hub wall boundary layer and probably exist in the form of a ring vortex since the hub is cylindrical in shape. Evidence of long eddies is clear from plots of $\rho_{uu}(\tau)$ in Figs. 7a, 8, and 9 and Table 2. The presence of the grid tends to reduce or eliminate the long eddies as seen in Fig. 7b and Table 2.

With all three boundary layers, the cross-correlation $[\rho_{vv}(\theta)]$ plots seem to indicate the presence of a thin as well as a ring-vortex-type of eddy as evidenced by nearly uniform values of $\rho_{vv}(\theta)$ even up to 50-deg circumferential-probe separation. In the artificial boundary layer, the cross-correlation becomes negative. This implies that the ring vortex eddy has changed its direction of rotation. Since this change in direction of rotation occurs at radial locations near the hub, it probably results from the O-ring trip near the nose cone of the hub. The cross-correlation curves for the fully developed boundary layer are similar to the natural boundary layer. The grid does not seem to bring about any substantial change in the tangential extent or length of the eddies as seen in Figs. 8 and 9 and Table 3.

Table 3 Circumferential integral scales (cms)

	No grid		Grid	
r/r_T	Large	Small	Large	Small
	Natural boundary layer (NBL)			
0.52	3.6	0.07	2.1	0.11
0.61	9.2	0.10	7.2	0.15
0.75	7.9	0.17	7.0	0.12
0.88	12.2	0.05	11.1	0.35
0.97	23.3	0.17	8.0	0.17
	Artificial boundary layer (ABL)			
0.52	0.50	0.29	0.32	0.21
0.58	0.71	0.29	0.86	0.21
0.70	3.60	0.48	3.10	0.36
0.84	0.32	0.45	0.38	0.17
0.97	4.00	0.39	ND	0.14
	Fully developed boundary layer (FDBL)			
0.52	1.80	0.34	1.80	0.33
0.58	1.20	NP	1.30	NP
0.70	ND	0.38	ND	0.35
0.84	1.10	NP	NP	0.45
0.97	6.10	0.46	5.60	0.43

NP = not present; ND = not determinable.

The turbulent energy spectra are derived from the hot-wire measurements at five radial locations. When these are normalized by total turbulence intensity (integrated over all the wave numbers), the data at all the five radii band as shown in Fig. 10, indicating that the energy spectrum is similar at all radii. The slope of the axial component and the tangential component of intensity in the range of wave numbers 10 to 100 m^{-1} is found to be -2.6.

Acoustic Measurements

The spectrum of background noise was taken without rotor, but with and without the auxiliary fan in operation. The background noise was low enough not to effect the radiated noise from the rotor. The directivity of the radiated sound was determined for the case of the 10-bladed rotor operating in the NBL with no grid. The radial position of the microphone was as shown in Fig. 3a. The results of this investigation are shown in Fig. 11. As seen, there are no lobes in

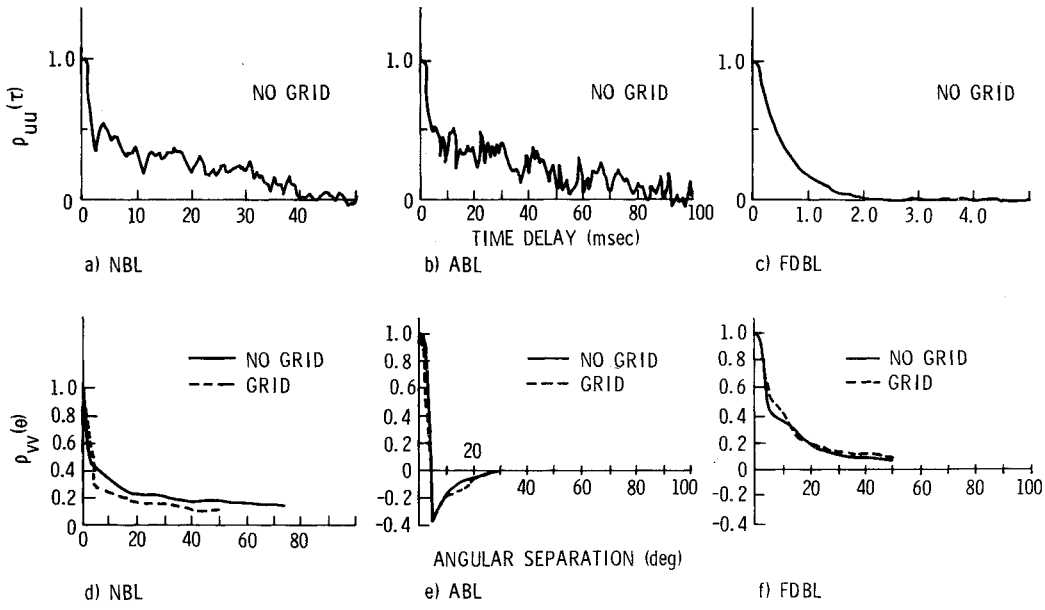

Fig. 9 Correlation curves, each boundary layer, $r/r_T = 0.58$, $\phi = 0.75$, 17 blades, 5440 rpm.

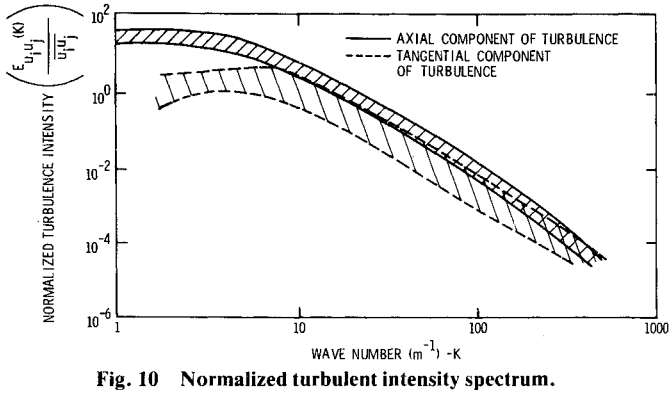

Fig. 10 Normalized turbulent intensity spectrum.

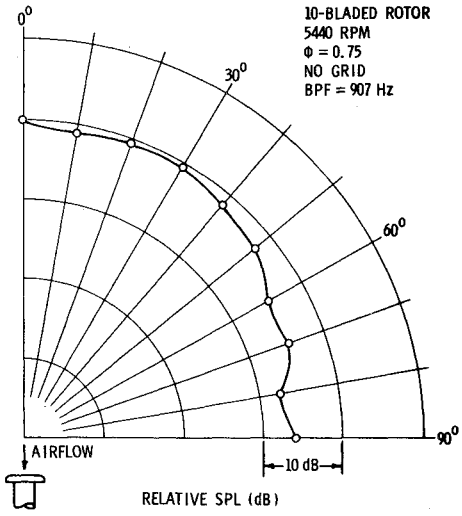

Fig. 11 Directivity measurements of SPL centered at BPF (907 Hz), 10 Hz bandwidth; NBL with 10-bladed rotor at 5440 rpm.

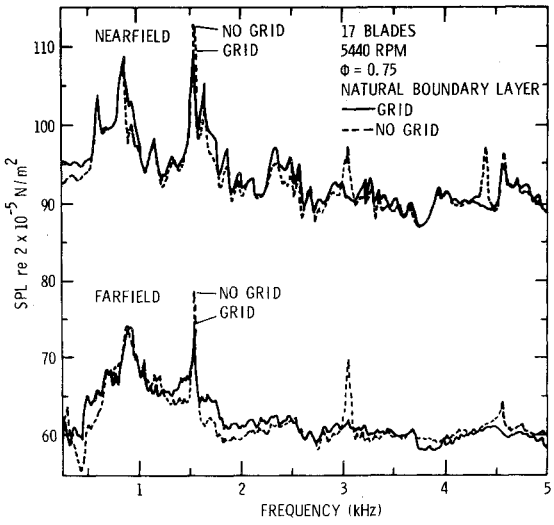

Fig. 12 Comparison of 17-bladed sound spectra with and without grid.

the directivity so that measurements with the microphone at only one angle were used for subsequent tests and the results considered representative for other angles.

The results of the sound measurements show a definite dependence on turbulence length scales. In Figs. 12 and 13, a comparison is made between the spectra obtained with the grid and no-grid (far- and near-field) for the natural boundary layer for both 10 and 17 blades. The decrease in the number and strength of harmonics above the blade-passing frequency (BPF) for the grid spectra is due to the large decrease in axial length scale caused by the grid. This is more pronounced for the 17-bladed case than the 10-bladed case. With grid, the second and subsequent harmonics disappear for the 17-bladed case, whereas for the 10-bladed case only the 4th and higher harmonics disappear. This is caused by higher blade loading in the case of the 10-bladed rotor. The results with varying flow coefficients (described later) tend to confirm this. The small rise in far-field broadband noise about blade-passing frequency can be attributed directly to the increase in turbulent intensity due to the presence of the grid. In Fig. 14, a comparison is made between the far-field noise spectra due to the 17- and 10-bladed rotors operating in the natural boundary-layer configuration with no grid. The two spectra were normalized with respect to frequency using $f/B\Omega$, where f is frequency, B is number of blades, and Ω is rotor rps. The turbulence properties were measured only for the 17-bladed rotor. They were assumed to be the same for the 10-bladed rotor, since the operating conditions and blade geometries

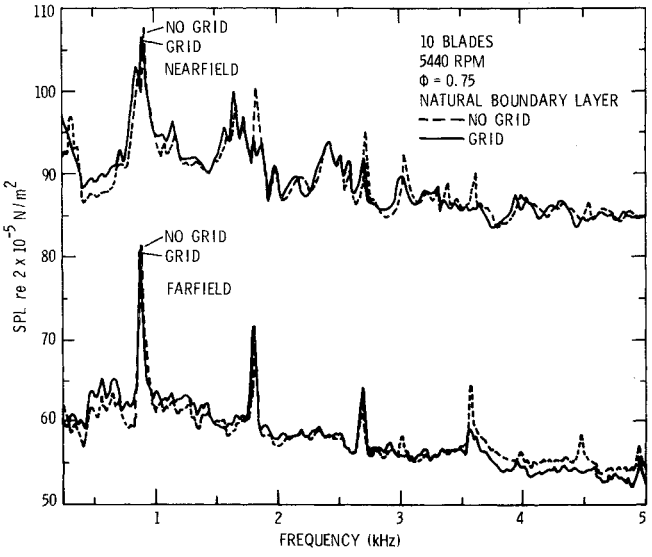

Fig. 13 Comparison of 10-bladed sound spectra with and without grid.

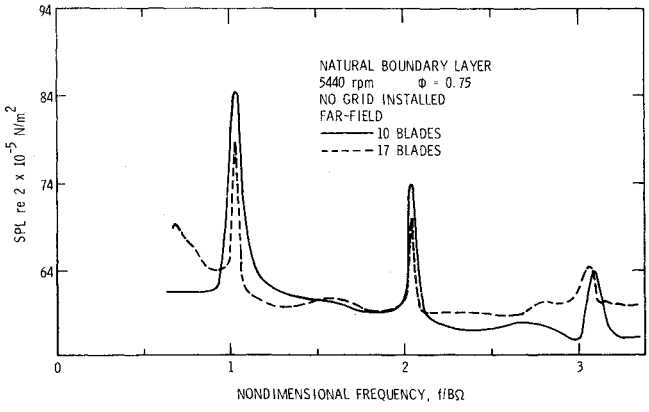

Fig. 14 Comparison of 17- and 10-bladed sound spectra without grid.

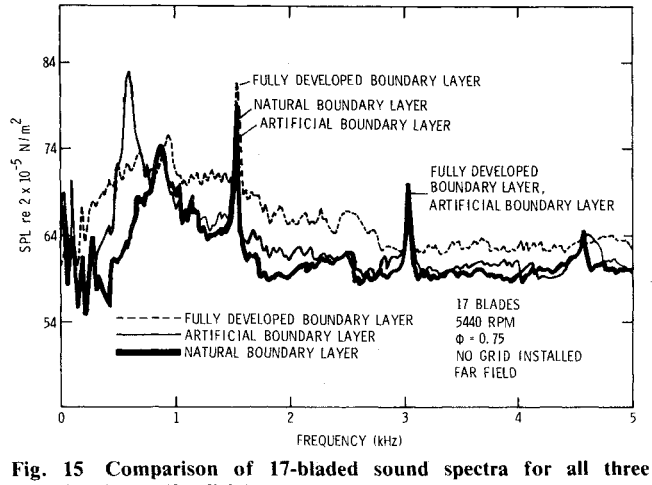

Fig. 15 Comparison of 17-bladed sound spectra for all three boundary layers (far-field).

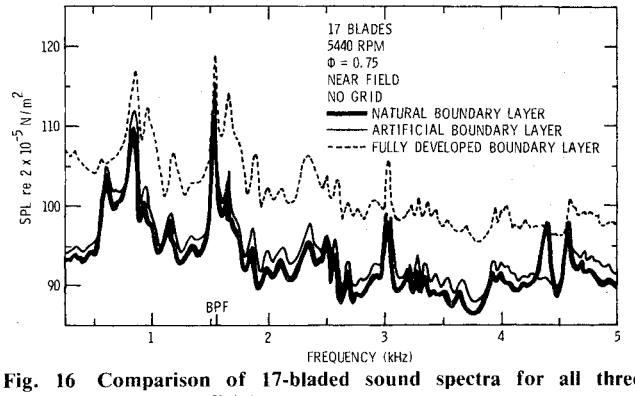

Fig. 16 Comparison of 17-bladed sound spectra for all three boundary layers (near-field).

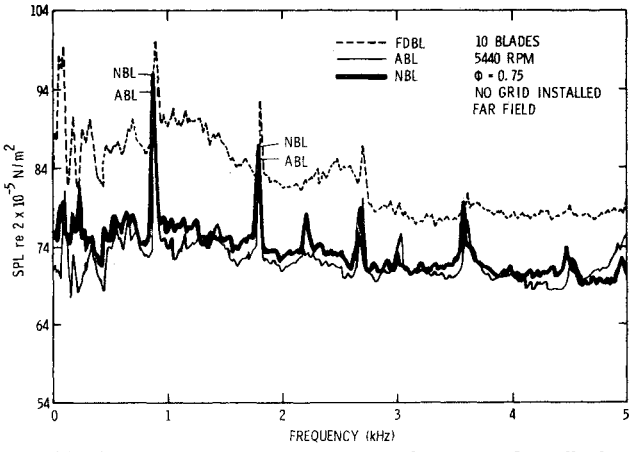

Fig. 17 Comparison of 10-bladed sound spectra for all three boundary layers (far-field).

were identical for both rotors. Hence, the only changes in the two configurations were the blade spacing and the steady loading. The unsteady aerodynamic transfer function is dependent on the spacing and is approximately proportional to the slope of the C_L vs incidence curve. Hence, using the flat-plate cascade theory, the increase in noise level due to a change in spacing, as shown in Fig. 14, can be estimated to be about 2 dB at BPF. The remaining increase for the 10-bladed rotor is presumably due to the change in L_x/S value with L_x fixed and S changing. This seems to qualitatively confirm Mani's[3] conclusion on the effect of L_x/S on noise level. The correlations developed in the next section of the paper also tend to confirm the dependence of L_x/S on the noise level.

In Figs. 15-18, the sound spectra for the two-rotor configurations are compared for the three different boundary layers. The corresponding BPF tone levels are tabulated in Table 1. A general increase in the broad-band noise level with increasing boundary-layer thickness is attributed to the increase in turbulence intensity for each boundary layer, and not to any mean velocity-gradient effect. The change in intensity between the NBL and ABL is not large, whereas there is a substantial increase in intensity for the FDBL case (Figs. 5 and 6).

The BPF tone is highest for the fully developed boundary layer. This is a consequence of the higher levels of turbulence intensity associated with the FDBL and is in conformity with the investigations reported in Refs. 1-3. Referring to Figs. 12 and 13 and Tables 2 and 3, it is apparent that the axial length scale has more influence on the number and strength of the higher harmonics of the BPF tone than on the strength of the BPF tone itself. The turbulence intensity has a major influence on the BPF tone noise. Hence, a small difference between the NBL and ABL-BPF peaks is seen (numerical values given in Table 1). The BPF noise level is highest for FDBL case with ABL being the lowest of the three. Referring to Tables 2 and 3, it is evident that the ABL has the longest axial length scale and shortest tangential length scale. The latter may have considerable influence in providing the lowest noise level at BPF for the artificial boundary layer. This seems to indicate the importance of tangential length scale (L_θ/S), which is less than unity at most radii for ABL case.

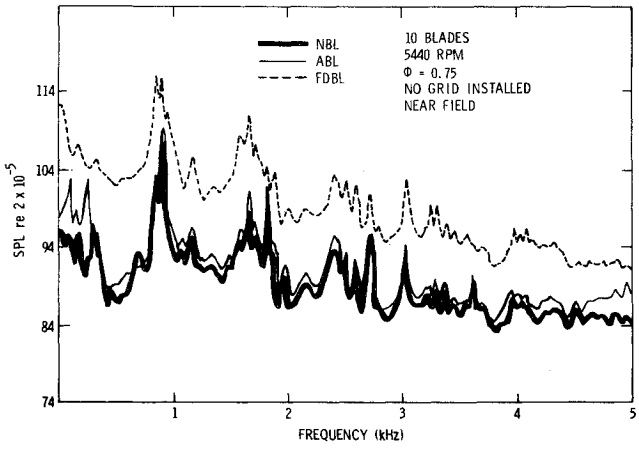

Fig. 18 Comparison of 10-bladed sound spectra for all three boundary layers (near-field).

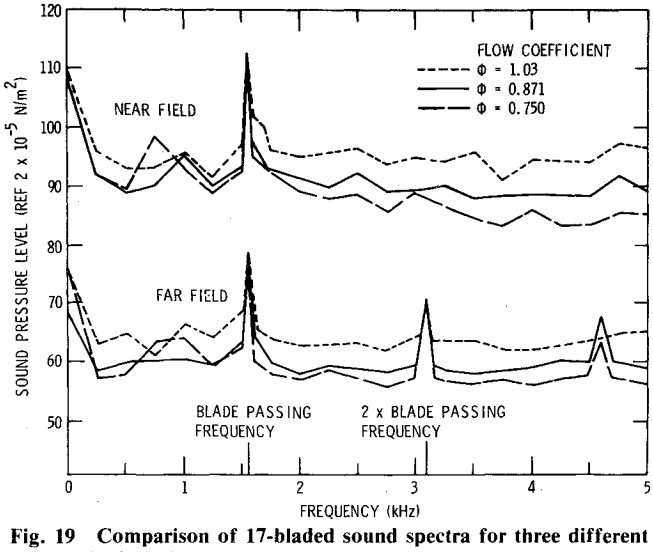

Fig. 19 Comparison of 17-bladed sound spectra for three different flow coefficients for the natural boundary layer.

Figure 19 shows the sound spectra for the natural boundary layer, no-grid configuration at three different flow coefficients: 0.75, 0.87 and 1.03. The broadband noise level rises with increasing flow coefficient, while the BPF tone is constant. The rise in broadband noise level is due to the increase in mean velocity and turbulence intensity associated with the increased flow coefficient. The mean velocity controls the blade loading and hence the aerodynamic transfer function, whereas the effect of turbulence intensity is similar to that discussed earlier. Hence, a change in flow coefficient corresponds to a change in steady blade loading. Figure 19 also indicates that changes in the steady blade loading affect the number of higher harmonics present. Similar measurements were not conducted for the ABL or FDBL. Further work in this area should be done.

Correlation and Discussion

Previous investigations, both theoretical and experimental, have indicated that the sound pressure varies as the square of the turbulence intensities and inversely as the square of the axial integral length scale for the rotor interacting with isotropic turbulence. In the present investigation, a different correlation has been found. The sound pressure varies as the square of turbulence intensities, but inversely as the ratio of axial integral length scale to the blade spacing. With the 10-bladed rotor operating with the grid, the proper mean inflow velocities could not be achieved, hence the results do not

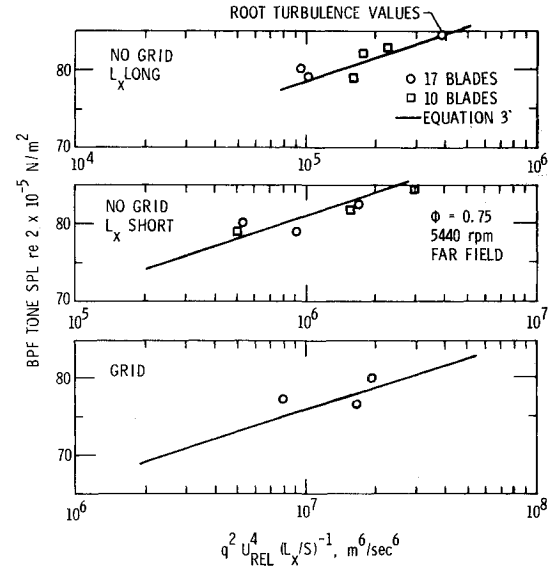

Fig. 20 Correlation between noise and turbulence data (root values).

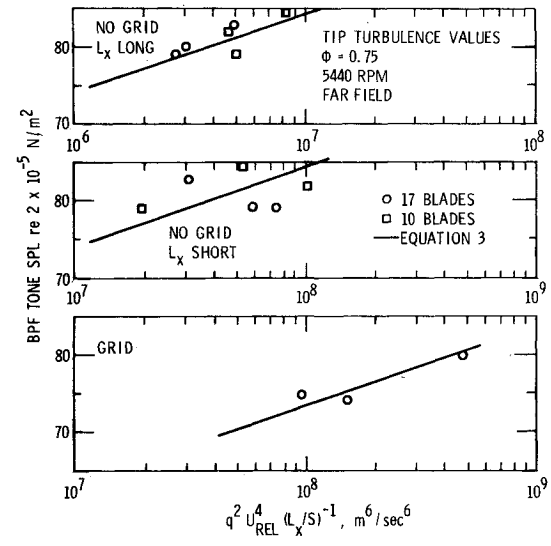

Fig. 21 Correlation between noise and turbulence data (tip values).

appear in the correlations. The correlating parameter is $\overline{q^2}U_{\text{rel}}^4 (L_x/S)^{-1}$, where $\overline{q^2}$ is the turbulence intensity normal to the blade, and L_x is the axial integral length scale. The far-field sound at BPF is correlated in Figs. 20 and 21 and follows the relation

$$\text{SPL} = (\text{SPL})_0 + 40\log U_{\text{rel}} + 10\log\overline{q^2} - 10\log(L_x/S) \quad (3)$$

where $(\text{SPL})_0$ is a constant base level.

The values of the turbulence properties are taken from near the hub and near the tip. Correlations with values at midradius are poor. This indicates that sound generation is primarily from the root and tip regions of the rotor which operates in the hub and outer wall boundary layers.

The main effect of the long axial length scale is on the number and strength of higher harmonics of the BPF. This is clearly shown in Figs. 12 and 13, where the sound spectra with and without the grid are compared. When the long scales are present (no-grid), the second and thrid harmonics are present. When only the small scales are present (grid) these disappear. Hanson[1] reached a similar conclusion saying that the long length scales are responsible for the spectral distribution of sound energy; that is, they lead to narrow peaks in the noise spectra.

No definite conclusions can be drawn with regard to the effect of the tangential scales on the sound spectrum. An interesting observation is that the tangential scales L_θ for the ABL were much less than the blade spacing S. The BPF levels for the ABL were lower than either the NBL or FDBL both of which had much higher L_θ/S ratios.

Conclusions

The following conclusions can be drawn from this study, which had the objective of understanding the relationship between boundary-layer inflow turbulence and the noise generated by its interaction with a blade row:

1) Two length scales of turbulence are found to exist simultaneously in the inflow of a static-fan facility with no grid installed, long and short scales in the axial direction, narrow and wide in the tangential direction. The long axial scale disappears with a grid present.

2) Turbulence intensities are found to be maximum at the outer wall with appreciable magnitudes found even at midradius where the turbulence is primarily from the freestream.

3) The controlling factors in noise generation are the turbulence intensity and length scale. An empirical relation (Eq. 3) has been developed between these turbulence properties and radiated noise levels. It does not seem to make any difference as to the source of the turbulence. Boundary layer and atmospheric turbulence have the same effects. Atmospheric turbulence does influence boundary-layer turbulence.

4) The long axial length scales appear to be a strong factor in determining the number and strength of BPF harmonics. Short axial length scales contribute primarily to the general broadband noise levels. These major differences between the effect of long and short length scales could possibly account for the discrepancies between inflight and static noise tests. Further evidence of this has been gained in private communication.

5) The correlation of the data indicate that the primary sources of sound radiated from the rotor appear to be the root and tip region. Since these regions often operate in boundary layers, boundary-layer turbulence can be an important source of radiated noise.

6) Mani's[3] prediction that with decreasing L_x/S (for nearly isotropic turbulence) the general noise level will increase and BPF peaks will broaden seems to be borne out by the comparison between 17- and 10-bladed rotor spectra with identical entry turbulence.

7) The measurements indicate that the noise level, particularly at BPF, depends on the tangential scales, but no quantitative conclusions can be drawn.

8) Changes in the blade loading affect the number of BPF tones present in the sound spectrum.

Acknowledgment

This research was carried out under the Naval Sea Systems Command General Hydromechanics Research Program Subproject SR 023 01 01, administered by the David W. Taylor Naval Ship Research and Development Center, Contract N00017-73-C-1418.

References

[1] Hanson, D. B., "Spectrum of Rotor Noise Caused by Atmospheric Turbulence," *Journal of Acoustical Society of America*, Vol. 56, July 1974, pp. 110-126.

[2] Robbins, B. and Lakshminarayana, B., "Effect of Inlet Turbulence on Compressor Noise," *Journal of Aircraft*, Vol. 11, May 1974, pp. 273-281.

[3] Mani, R., "Noise Due to Interaction of Inlet Turbulence with Isolated Stators and Rotors," *Journal of Sound and Vibration*, Vol. 17, Feb. 1971, pp. 251-260.

[4] Sevik, M., "Sound Radiation from a Subsonic Rotor Subjected to Turbulence," in *Fluid Mechanics, Acoustics, and Design of Turbomachinery*, Part 2, edited by B. Lakshminarayana, W. R. Britsch, and W. S. Gearhart, NASA SP 304, 1974, pp. 493-511.

[5] Lakshminarayana, B., "Influence of Turbulence on Fan Noise," *Proceedings of the Workshop on Ventilation System Cooling Fan Noise*, Naval Sea Systems Command, edited by M. Sevik and J. Pierpoint, 1976, pp. G1-G34.

[6] Feiler, C. E. and Conrad, E. W., "Fan Noise from Turbofan Engines," *Journal of Aircraft*, Vol. 13, Feb. 1976, pp. 128.

[7] Moiseev, N., Lakshminarayana, B., and Thompson, D. E., "Noise Due to Interaction of Boundary Layer Turbulence with a Marine Propulsor or an Aircraft Compressor," Applied Research Laboratory, The Pennsylvania State University, TM 76-258, 1977.